6986 *Inorg. Chem.* **2010**, *49*, 6986–6993
DOI: 10.1021/ic1008297

Inorganic Chemistry
Article

$A_3V_5O_{14}$ (A = K^+, Rb^+, or Tl^+), New Polar Oxides with a Tetragonal Tungsten Bronze Related Structural Topology: Synthesis, Structure, and Functional Properties

Jeongho Yeon, Sang-Hwan Kim, and P. Shiv Halasyamani*

Department of Chemistry, University of Houston, 136 Fleming Building, Houston, Texas 77204-5003

Received April 27, 2010

Three polar noncentrosymmetric (NCS) oxide materials, $A_3V_5O_{14}$ (A = K^+, Rb^+, or Tl^+), have been synthesized by hydrothermal and conventional solid state techniques. Their crystal structures and functional properties (second-harmonic generation, piezoelectricity, and polarization) have been determined. The iso-structural materials exhibit a layered structural topology that consists of corner-sharing VO_4 tetrahedra and VO_5 square pyramids. The layers stack parallel to the *c*-axis direction and are separated by the K^+, Rb^+, or Tl^+ cations. Powder second-harmonic generation (SHG) measurements using 1064 nm radiation indicate the materials exhibit moderate SHG efficiencies of $\sim 100 \times \alpha$-SiO_2. Additional SHG measurements, that is, particle size versus SHG efficiency, indicate the materials are type-I phase-matchable. Converse piezoelectric measurements for $K_3V_5O_{14}$, $Rb_3V_5O_{14}$, and $Tl_3V_5O_{14}$ revealed d_{33} values of 28, 22, and 26 pm/V, respectively. Pyroelectric measurements, that is, temperature-dependent polarization measurements, resulted in pyroelectric coefficients of −2.2, −2.9, and −2.8 $\mu C/m^2 \cdot K$ at 65 °C, for $K_3V_5O_{14}$, $Rb_3V_5O_{14}$, and $Tl_3V_5O_{14}$ respectively. Frequency-dependent polarization measurements confirmed that all of the materials are nonferroelectric, consistent with our first principle density functional theory (DFT) electronic structure calculations. Infrared, UV−vis, thermogravimetric, and differential scanning calorimetry measurements were also performed. Crystal data: $K_3V_5O_{14}$, trigonal, space group $P31m$ (No. 157), $a = 8.6970(16)$ Å, $c = 4.9434(19)$ Å, $V = 323.81(15)$, and $Z = 1$; $Rb_3V_5O_{14}$, trigonal, space group $P31m$ (No. 157), $a = 8.7092(5)$ Å, $c = 5.2772(7)$ Å, $V = 346.65(5)$, and $Z = 1$; $Tl_3V_5O_{14}$, trigonal, space group $P31m$ (No. 157), $a = 8.7397(8)$ Å, $c = 5.0846(10)$ Å, $V = 336.34(8)$, and $Z = 1$.

Introduction

Polar materials, that is, those that exhibit a macroscopic dipole moment, are of topical interest attributable to their technologically relevant functional properties, for example, ferroelectricity, pyroelectricity, multiferroic behavior, and so forth.[1−3] For a material to be considered polar, it *must* crystallize in one of 10 polar crystal classes, (1, 2, 3, 4, 6, m, mm2, 3 m, 4 mm, or 6 mm).[4] The two most common functional properties associated with polarity are ferroelectricity and pyroelectricity. With the former, the observed polarization may be switched in the presence of an external electric field. It is this "switchablility" that is the basis for the technological relevance of ferroelectric materials.[5] With the latter, the polarization is not switchable; however, the magnitude of the spontaneous polarization varies as a function of temperature.[1,6] Thus all ferroelectrics are pyroelectrics, but the converse is not true. With respect to synthesizing new polar inorganic materials, as well as noncentrommetric materials as a whole, a variety of strategies have been proposed.[7−36] We have focused on using cations susceptible to

---

*To whom correspondence should be addressed. E-mail: psh@uh.edu.

(1) Lang, S. B. *Phys. Today* **2005**, *58*, 31.

(2) Ok, K. M.; Chi, E. O.; Halasyamani, P. S. *Chem. Soc. Rev.* **2006**, *35*, 710.

(3) Khomskii, D. I. *Physics* **2009**, *2*, 20.

(4) Hahn, T. *International Tables for Crystallography, Vol. A, Space Group Symmetry*; Kluwer Academic: Dordrecht, The Netherlands, 2006; Vol. *A*.

(5) Auciello, O.; Scott, J. F.; Ramesh, R. *Phys. Today* **1998**, *51*, 22.

(6) Lang, S. B., Das-Gupta., D. K. In *Handbook of Advanced Electronic and Photonic Materials and Devices*; Nalwa, H. S., Ed.; Academic Press: San Francisco, 2001; Vol. *4*, p 1.

(7) Hwu, S.-J.; Ulutagay-Kartin, M.; Clayhold, J. A.; Mackay, R.; Wardojo, T. A.; O'Connor, C. J.; Kraweic, M. *J. Am. Chem. Soc.* **2002**, *124*, 12404.

(8) Huang, Q.; Hwu, S.-J. *Inorg. Chem.* **2003**, *42*, 655.

(9) Mo, X.; Hwu, S.-J. *Inorg. Chem.* **2003**, *42*, 3978.

(10) Mo, X.; Ferguson, E.; Hwu, S.-J. *Inorg. Chem.* **2005**, *44*, 3121.

(11) Queen, W. L.; West, J. P.; Hwu, S.-J.; VanDerveer, D. G.; Zarzyczny, M. C.; Pavlick, R. A. *Angew. Chem., Int. Ed.* **2008**, *47*, 3791.

(12) Heier, K. R.; Norquist, A. J.; Halasyamani, P. S.; Duarte, A.; Stern, C. L.; Poeppelmeier, K. R. *Inorg. Chem.* **1999**, *38*, 762.

(13) Welk, M. E.; Norquist, A. J.; Stern, C. L.; Poeppelmeier, K. R. *Inorg. Chem.* **2000**, *39*, 3946.

(14) Welk, M. E.; Norquist, A. J.; Stern, C. L.; Poeppelmeier, K. R. *Inorg. Chem.* **2001**, *40*, 5479.

(15) Welk, M. E.; Norquist, A. J.; Arnold, F. P.; Stern, C. L.; Poeppelmeier, K. R. *Inorg. Chem.* **2002**, *41*, 5119.

(16) Izumi, H. K.; Kirsch, J. E.; Stern, C. L.; Poeppelmeier, K. R. *Inorg. Chem.* **2005**, *44*, 884.

(17) Marvel, M. R.; Lesage, J.; Baek, J.; Halasyamani, P. S.; Stern, C. L.; Poeppelmeier, K. R. *J. Am. Chem. Soc.* **2007**, *129*, 13963.

(18) Kepert, C. J.; Rosseinsky, M. J. *Chem. Commun.* **1998**, 31.

(19) Prior, T. J.; Rosseinsky, M. J. *Chem. Commun.* **2001**, 495.

(20) Prior, T. J.; Rosseinsky, M. J. *Inorg. Chem.* **2003**, *42*, 1564.

(21) Rosseinsky, M. J. *Microporous Mesoporous Mater.* **2004**, *73*, 15.

second-order Jahn–Teller (SOJT) distortions,[37–43] octahedrally coordinated d^0 transition metal cations and cations with a lone-pair. In doing so, we have synthesized and characterized a host of polar materials.[44–55] When the individual polar polyhedra, that is, d^0 transition metal octahedra and lone-pair polyhedra, are aligned, the material exhibits a macroscopic polarization. Thus, the origin and magnitude of the aforementioned functional properties are critically dependent on the individual asymmetric units as well as their alignment in the crystal structure. It remains a challenge, however, to control the alignment and to reliably predict the strength of the functional properties.

A structural topology that is amenable to polarity is the tetragonal tungsten bronze (TTB) structure.[56,57] TTB oxides have been studied extensively attributable to their fascinating structural chemistry and technologically relevant physical properties.[56–61] The TTB structure consists of a three-dimensional corner-sharing framework of MO_6 octahedra (M = Ti, Nb, Ta, W, Fe, Co, etc.) that contain interstitial sites where a variety of metal cations (alkali, alkaline earth, and lanthanide) may reside. In this paper we report on the synthesis, structure, and functional properties of three polar oxides, $A_3V_5O_{14}$ (A = K^+, Rb^+, or Tl^+), that exhibit a TTB layer-like topology. $K_3V_5O_{14}$ was first reported in 1959 by Bystrom,[62] with a more thorough crystal structure published in 1994.[63] With the latter, however, no physical properties were reported. In a more recent publication on $K_3V_5O_{14}$, powder second-harmonic generation (SHG) measurements were reported that suggested a very large SHG efficiency, $\sim 20 \times$ KDP or $\sim 800 \times \alpha\text{-}SiO_2$.[64] This efficiency, nearly double that of $BaTiO_3$, seemed inconsistent with the structural topology and cation coordination environments. To confirm the SHG efficiency, and investigate structure–property relationships, we resynthesized $K_3V_5O_{14}$ as well as the new materials $Rb_3V_5O_{14}$ and $Tl_3V_5O_{14}$. We were unable to synthesize $Cs_3V_5O_{14}$ attributable to the stability of $CsVO_3$[65] and $Cs_2V_4O_{14}$.[66]

In this paper, we report on the synthesis, structure, and functional properties of $K_3V_5O_{14}$, $Rb_3V_5O_{14}$, and $Tl_3V_5O_{14}$. We show that the previously reported SHG efficiency for $K_3V_5O_{14}$ is erroneously high through a careful examination of its crystal structure. In addition, although all three materials are polar, they do not exhibit ferroelectric behavior, that is, their polarization is not switchable. Finally, we discuss structure–property relationships, as well as present theoretical calculations that provide insight into the functional properties of the reported materials.

Experimental Section

Reagents. KNO_3 (Alfa Aesar, 99%), $RbNO_3$ (Alfa Aesar, 99%), Tl_2CO_3 (Alfa Aesar, 99.9+%), and V_2O_5 (Aldrich, 99+%) were used as received.

Synthesis. Single crystals of $K_3V_5O_{14}$ and $Rb_3V_5O_{14}$ were grown from reactions where 0.120 g (0.247 g) (1.19 mmol (1.67 mmol)) of KNO_3 ($RbNO_3$) and 0.180 g (0.253 g) (1.00 mmol (1.40 mmol)) of V_2O_5 were placed in a platinum crucible. The crucible was gradually heated to 600 °C in air, held for 24 h, and then cooled slowly to room temperature (RT) at a rate of 6 °C h^{-1}. For $K_3V_5O_{14}$, red block-shaped crystals were found as a pure phase, whereas with $Rb_3V_5O_{14}$ red block-shaped crystals were recovered in ~11% yield based upon V_2O_5. $Tl_3V_5O_{14}$ was hydrothermally synthesized by combining 0.422 g (0.900 mmol) of Tl_2CO_3, 0.327 g (1.80 mmol) of V_2O_5, and 0.251 g (4.05 mmol) of H_3BO_3 with 4 mL of H_2O in a 23 mL Teflon-lined autoclave. The autoclave was closed, gradually heated to 230 °C, held for 48 h, and cooled slowly to room temperature at a rate of 6 °C h^{-1}. The mother liquor was decanted, and the products were recovered by filtration and washed with excess distilled water and acetone. Red multifaceted crystals, subsequently determined to be $Tl_3V_5O_{14}$, were recovered in ~20% yield based on V_2O_5.

Bulk samples of $K_3V_5O_{14}$, $Rb_3V_5O_{14}$ and $Tl_3V_5O_{14}$ were prepared by conventional solid-state methods. Separate stoichiometric amounts of KNO_3 (0.400 g, 3.96 mmol), $RbNO_3$ (0.584 g, 3.96 mmol), Tl_2CO_3 (0.928 g, 1.98 mmol), and V_2O_5 (0.600 g, 3.30 mmol) were thoroughly ground and pressed into pellets. The pellets were placed in alumina crucibles and were heated to 380 °C in air, held for 4 days, and then cooled to RT. The pellets were reground three to five times, heated and cooled as before. The materials were

---

(22) Bradshaw, D.; Claridge, J. B.; Cussen, E. J.; Prior, T. J.; Rosseinsky, M. J. *Acc. Chem. Res.* **2005**, *38*, 273.

(23) Ingleson, M. J.; Bacsa, J.; Rosseinsky, M. J. *Chem. Commun.* **2007**, 3036.

(24) Ingleson, M. J.; Barrio, J. P.; Bacsa, J.; Dickinson, C.; Park, H.; Rosseinsky, M. J. *Chem. Commun.* **2008**, 1287.

(25) Lin, W.; Evans, O. R.; Xiong, R.-G.; Wang, Z. *J. Am. Chem. Soc.* **1998**, *120*, 13272.

(26) Evans, O. R.; Lin, W. *Acc. Chem. Res.* **2002**, *35*, 511.

(27) Lee, S. J.; Lin, W. *J. Am. Chem. Soc.* **2002**, *124*, 4554.

(28) Cui, Y.; Lee, S. J.; Lin, W. *J. Am. Chem. Soc.* **2003**, *125*, 6014.

(29) Cui, Y.; Ngo, H. L.; White, P. S.; Lin, W. *Chem. Commun.* **2003**, 994.

(30) Jiang, H.; Lin, W. *J. Am. Chem. Soc.* **2003**, *125*, 8084.

(31) Kesanli, B.; Lin, W. *Coord. Chem. Rev.* **2003**, *246*, 305.

(32) Lee, S. J.; Lin, W. *Acc. Chem. Res.* **2008**, *41*, 521.

(33) Kong, F.; Huang, S.-P.; Sun, Z.-M.; Mao, J.-G.; Cheng, W.-D. *J. Am. Chem. Soc.* **2006**, *128*, 7750.

(34) Jiang, H.-L.; Huang, S.-P.; Fan, Y.; Mao, J.-G.; Cheng, W.-D. *Chem—Eur. J.* **2008**, *14*, 1972.

(35) Hu, T.; Qin, L.; Kong, F.; Zhou, Y.; Mao, J.-G. *Inorg. Chem.* **2009**, *48*, 2193.

(36) Sun, C.-F.; Hu, C.-L.; Xu, X.; Ling, J.-B.; Hu, T.; Kong, F.; Long, X. F.; Mao, J.-G. *J. Am. Chem. Soc.* **2009**, *131*, 9486.

(37) Opik, U.; Pryce, M. H. L. *Proc. R. Soc. London, Ser. A* **1957**, *238*, 425.

(38) Bader, R. F. W. *Mol. Phys.* **1960**, *3*, 137.

(39) Bader, R. F. W. *Can. J. Chem.* **1962**, *40*, 2140.

(40) Pearson, R. G. *J. Am. Chem. Soc.* **1969**, *91*, 4947.

(41) Pearson, R. G. *THEOCHEM* **1983**, *12*, 25.

(42) Wheeler, R. A.; Whangbo, M. H.; Hughbanks, T.; Hoffmann, R.; Burdett, J. K.; Albright, T. A. *J. Am. Chem. Soc.* **1986**, *108*, 2222.

(43) Goodenough, J. B. *Annu. Rev. Mater. Sci.* **1998**, *28*, 1.

(44) Goodey, J.; Broussard, J.; Halasyamani, P. S. *Chem. Mater.* **2002**, *14*, 3174.

(45) Ra, H.-S.; Ok, K. M.; Halasyamani, P. S. *J. Am. Chem. Soc.* **2003**, *125*, 7764.

(46) Ok, K. M.; Halasyamani, P. S. *Angew. Chem., Int. Ed.* **2004**, *43*, 5489.

(47) Chi, E. O.; Ok, K. M.; Porter, Y.; Halasyamani, P. S. *Chem. Mater.* **2006**, *18*, 2070.

(48) Sivakumar, T.; Ok, K. M.; Halasyamani, P. S. *Inorg. Chem.* **2006**, *45*, 3602.

(49) Kim, J.-H.; Baek, J.; Halasyamani, P. S. *Chem. Mater.* **2007**, *19*, 5637.

(50) Chang, H. Y.; Sivakumar, T.; Ok, K. M.; Halasyamani, P. S. *Inorg. Chem.* **2008**, *47*, 8511.

(51) Kim, J.-H.; Baek, J.; Halasyamani, P. S. *Chem. Mater.* **2008**, *20*, 3542.

(52) Chang, H. Y.; Kim, S.-H.; Ok, K. M.; Halasyamani, P. S. *Chem. Mater.* **2009**, *21*, 1654.

(53) Chang, H.-Y.; Kim, S.-H.; Ok, K. M.; Halasyamani, P. S. *J. Am. Chem. Soc.* **2009**, *131*, 6865.

(54) Kim, S.-H.; Yeon, J.; Halasyamani, P. S. *Chem. Mater.* **2009**, *21*, 5335.

(55) Chang, H. Y.; Kim, S. W.; Halasyamani, P. S. *Chem. Mater.* **2010**, in press.

(56) Jamieson, P. B.; Abrahams, S. C. *Acta Crystallogr., Sect. B* **1968**, *24*, 984.

(57) Jamieson, P. B.; Abrahams, S. C.; Bernstein, J. L. *J. Chem. Phys.* **1969**, *50*, 4352.

(58) Lenzo, P. V.; Spenser, E. G.; Ballman, A. A. *Appl. Phys. Lett.* **1967**, *11*, 23.

(59) Itoh, Y.; Iwasaki, H. *J. Phys. Chem. Solids* **1972**, *34*, 1639.

(60) Neurgaonkar, R. R.; Nelson, J. G.; Oliver, J. R.; Cross, L. E. *Mater. Res. Bull.* **1990**, *25*, 959.

(61) Neurgaonkar, R. R.; Nelson, J. G.; Oliver, J. R. *Mater. Res. Bull.* **1992**, *27*, 677.

(62) Bystrom, A. M.; Evans, H. T., Jr. *Acta Chem. Scand.* **1959**, *13*, 377.

(63) Evans, H. T., Jr.; Brusewitz, A. M. *Acta Chem. Scand.* **1994**, *48*, 533.

(64) Li, G.; Su, G.; Zhuang, X.; Li, Z.; He, Y. *Opt. Mater.* (*Amsterdam, Neth.*) **2005**, *27*, 539.

(65) Hawthorne, F. C.; Calvo, C. *J. Solid State Chem.* **1977**, *22*, 157.

(66) Oka, Y.; Saito, F.; Yao, T.; Yamamoto, N. *J. Solid State Chem.* **1997**, *134*, 52.

Table 1. Crystallographic Data for $A_3V_5O_{14}$ (A = Rb^+, and Tl^+)

formula	$Rb_3V_5O_{14}$	$Tl_3V_5O_{14}$
fw	735.11	1091.81
T(K)	296.0(2)	296.0(2)
crystal system	trigonal	trigonal
space group	$P31m$ (No. 157)	$P31m$ (No. 157)
a (Å)	8.7092(5)	8.7397(8)
c (Å)	5.2772(7)	5.0846(10)
α (deg)	90	90
γ (deg)	120	120
V (Å^3)	346.65(5)	336.34(8)
Z	1	1
ρ_{calcd} (g/cm^3)	3.521	5.390
μ(mm^{-1})	13.776	39.173
2 θ_{max} (deg)	57.98	57.44
R (int)	0.0420	0.0267
GOF (F^2)	1.109	1.096
$R(F)^a$	0.0174	0.0156
$R_w(F_o^2)^b$	0.0435	0.0309
Flack parameter	0.000(8)	−0.004(8)

$^a R(F) = \sum||F_o| - |F_c||/\sum|F_o|$. $^b R_w(F_o^2) = [\sum w(F_o^2 - F_c^2)^2/\sum w(F_o^2)^2]^{1/2}$.

Table 2. Atomic Coordinates and Equivalent Isotropic Displacement Parameters (Å^2) for $A_3V_5O_{14}$ (A = Rb^+, and Tl^+).^{a}

	x	y	z	$U_{eq}{}^b$
		$Rb_3V_5O_{14}$		
Rb(1)	0.6122(1)	0	0.2144(1)	0.022(1)
V(1)	0.3333	0.6667	0.6912(2)	0.012(1)
V(2)	0.2305(1)	0	0.7067(2)	0.014(1)
O(1)	0.3333	0.6667	0	0.021(1)
O(2)	0.22526(5)	0	0.0083(7)	0.026(1)
O(3)	0.8326(4)	0	0.6470(8)	0.023(1)
O(4)	0.1698(3)	0.4610(3)	0.5797(5)	0.017(1)
		$Tl_3V_5O_{14}$		
Tl(1)	0.6085(1)	0	0.2089(3)	0.024(1)
V(1)	0.3333	0.6667	0.6785(3)	0.011(1)
V(2)	0.2285(1)	0	0.6869(3)	0.013(1)
O(1)	0.3333	0.6667	0	0.024(2)
O(2)	0.2464(7)	0	0	0.025(1)
O(3)	0.8324(6)	0	0.6188(11)	0.021(1)
O(4)	0.1692(4)	0.4616(5)	0.5616(7)	0.017(1)

^{a} Equivalent atomic coordinates are presented. ^{b} U_{eq} is defined as one-third of the trace of the orthogonalized U_{ij} tensor.

determined to be pure by powder X-ray diffraction (see Supporting Information, Figure S1 and Powder Diffraction Section). We also attempted to synthesize the Li^+, Na^+, and Cs^+ analogues, but were unsuccessful. With Li^+ and Na^+, it is clear that the 10-coordinate environment observed in the K^+, Rb^+, and Tl^+ phases (see Crystal Structure Description) is too large for these cations, whereas for Cs^+ a mixture of $CsVO_3$[65] and $Cs_2V_4O_{11}$[66] is always found.

Single-Crystal X-ray Diffraction. A red block-shaped crystal (0.13 × 0.10 × 0.07 mm^3) of $K_3V_5O_{14}$, a red block-shaped crystal (0.04 × 0.04 × 0.04 mm^3) of $Rb_3V_5O_{14}$, and a red multifaceted crystal (0.01 × 0.01 × 0.01 mm^3) of $Tl_3V_5O_{14}$ were used for single-crystal data collection. Data were collected using a Siemens SMART diffractometer equipped with a 1K CCD area detector using graphite-monochromated Mo Kα radiation. A hemisphere of data was collected using a narrow-frame method with scan widths of 0.30° in ω and an exposure time of 10 s, 50 s, and 40 s per frame for $K_3V_5O_{14}$, $Rb_3V_5O_{14}$, and $Tl_3V_5O_{14}$, respectively. The data were integrated using the Siemens SAINT program,[67] with the intensities corrected for Lorentz polarization, air absorption, and absorption attributable to the variation in the path length through the detector faceplate. Multiscans for $K_3V_5O_{14}$ and ψ-scans for $Rb_3V_5O_{14}$ and $Tl_3V_5O_{14}$ were used for the absorption correction on the hemisphere of data. All of the data were solved by direct methods using SHELXS-97 and refined using SHELXL-97.[68,69] All of the atoms were refined with anisotropic thermal parameters and converged for $I > 2\sigma(I)$ (Tables 1, 2). All calculations were performed using the WinGX-98 crystallographic software package.[70]

Powder X-ray Diffraction. Powder X-ray diffraction (PXRD) data of the materials were collected using a PANalytical X'Pert PRO diffractometer operating with Cu−Kα radiation. The data were taken in the 2θ range of 5°−90° with a step size of 0.008° and a fixed time of 0.3 s. No impurities were observed, and the calculated and experimental PXRD patterns are in excellent agreement (see Supporting Information, Figure S1).

Infrared (IR) Spectroscopy. Infrared spectra were recorded on a Matteson FT-IR 5000 spectrometer in the 400−4000 cm^{-1} range (see Supporting Information, Figure S2).

UV−vis Diffuse Reflectance Spectroscopy. UV−vis diffuse reflectance spectra were collected on a Varian Cary 500 scan UV−vis−NIR spectrophotometer over the spectral range 200−1500 nm at RT. Poly-(tetrafluoroethylene) was used as a reference material. Reflectance spectra were converted to absorbance with the Kubelka−Munk function[71,72] (see Supporting Information, Figure S3).

Thermogravimetric Analysis (TGA). Thermogravimetric analyses were carried out on a TGA 951 thermogravimetric analyzer (TA Instruments). The sample was placed into a platinum crucible and heated under air at a rate of 10 °C min^{-1} to 900 °C (see Supporting Information, Figure S4).

Differential Scanning Calorimetry Analysis (DSC). Differential scanning calorimetry (DSC) analysis was performed on an EXSTAR 6000 Differential Scanning Calorimeter (SII Nano Technology Inc.). Approximately 10 mg of the samples were placed into an aluminum pan covered by an aluminum lid, heated to 500 °C, and then cooled at a rate of 10 °C min^{-1} to RT under flowing air. Alumina was used as the reference during the measurements (see Supporting Information, Figure S4).

Second Harmonic Generation. Powder SHG measurements were performed on a modified Kurtz-NLO system[73] using a pulsed Nd:YAG laser with a wavelength of 1064 nm. A detailed description of the equipment and methodology has been published elsewhere.[2] As the powder SHG efficiency has been shown to depend strongly on particle size,[73] the reported materials were ground and sieved into distinct particle size ranges (< 20, 20−45, 45−63, 63−75, 75−90, > 90 μm). Relevant comparisons with known SHG materials were made by grinding and sieving crystalline α-SiO_2 and $LiNbO_3$ into the same particle size ranges. No index matching fluid was used in any of the experiments.

Piezoelectric Measurements. Converse piezoelectric measurements were performed using a Radiant Technologies RT66A piezoelectric test system with a TREK (model 609E-6) high voltage amplifier, Precision Materials Analyzer, Precision High Voltage Interface, and MTI 2000 Fotonic Sensor. The samples were pressed into pellets (~1.3 cm diameter, ~1 mm thick) and sintered at 360 °C for 7 days. Silver paste was applied to both sides of the pellets, and the pellets were cured at 200 °C for 12 h. The same pellets were also used in polarization measurements (see below).

Polarization Measurements. The polarization was measured on a Radiant Technologies RT66A ferroelectric test system with a TREK high-voltage amplifier between RT and 165 °C in a

---

(67) *SAINT, Program for Area Detector Absorption Correction*, 4.05; Siemens Analytical X-ray Systems: Madison, WI, 1995.

(68) Sheldrick, G. M. *SHELXS-97, A program for automatic solution of crystal structures*; University of Goettingen: Goettingen, Germany, 1997.

(69) Sheldrick, G. M. *SHELXS-97, A program for Crystal Structure Refinement*; University of Goettingen: Goettingen, Germany, 1997.

(70) Farrugia, L. J. *J. Appl. Crystallogr.* **1999**, *32*, 837.

(71) Kubelka, P.; Munk, F. *Z. Tech. Phys.* **1931**, *12*, 593.

(72) Tauc, J. *Mater. Res. Bull.* **1970**, *5*, 721.

(73) Kurtz, S. K.; Perry, T. T. *J. Appl. Phys.* **1968**, *39*, 3798.

Delta 9023 environmental test chamber. The unclamped pyroelectric coefficient, defined as dP/dT (change in polarization with respect to the change in temperature), was determined by measuring the polarization as a function of temperature. A detailed description of the methodology used has been published elsewhere.[2] To measure any possible ferroelectric behavior, the polarization was measured at RT under a static electric field from 10−14 kV/cm between 1000−4000 Hz. For the pyroelectric measurements, the polarization was measured statically from RT to 165 °C in 20 °C increments, with an electric field of 7−12 kV/cm. The temperature was allowed to stabilize before the polarization was measured.

Electronic Structure Calculations. First principles density functional theory (DFT) electronic band structure calculations were performed using the plane-wave pseudopotential and tight-binding linear muffin-tin orbital (TB-LMTO) methods. Norm-conserving Martins−Troullier (MT) pseudopotentials generated from FHI-98 code were utilized with a generalized gradient approximation (GGA) for the exchange-correlation corrections, as implemented in the Quantum ESPRESSO (4.0.1 version) package.[74] A plane wave energy cutoff of 37 Ry was fixed. A Gaussian smearing of 0.01 Ry for Brillouin zone integrations was adopted with a 4 × 4 × 6 k-point mesh in the unit cell. TB-LMTO calculations were also performed within the atomic sphere approximation (ASA). The von Barth-Hedin local exchange-correlation potential was used for the local density approximation (LDA). The radial scalar relativistic Dirac equation was solved for obtaining the partial waves. A total of 9 and 10 empty spheres were necessary to achieve space filling for $K_3V_5O_{14}$ and $Rb_3V_5O_{14}$, and for $Tl_3V_5O_{14}$ respectively. A total of 40 irreducible k-points from 6 × 6 × 4 grid was used for Brillouin zone integrations by tetrahedron method. The basis set consisted of K-4s/[4p], Rb-5s/[5p]/[4d]/[4*f*], Tl-6s/6p/[5d]/[5*f*], V-3d/4s/4p/ and O-2s/2p orbitals where the orbital in bracket was treated with the downfolding technique. Total energy changes of less than 10^{-5} Ry indicated self-consistency. For all of the structural figures and electronic structure calculation results, the program VESTA was used.[75]

Results and Discussion

Structures. The crystal structure of $A_3V_5O_{14}$ (A = K^+, Rb^+, and Tl^+) is shown in Figures 1a and 1b. All three materials exhibit two-dimensional (2D) cationic layers of $(V_5O_{14})^{3+}$ that are composed of corner shared VO_4 tetrahedra and VO_5 square pyramids. The 2D layers stack parallel to the *c*-direction, with A^+ cations residing between the layers. There are two crystallographically unique vanadium sites, hereafter referred to as V(1) and V(2) that have tetrahedral and square pyramidal coordination environments respectively. Three corner-shared $V(2)O_5$ square pyramids form a $V(2)_3O_{12}$ unit that is connected to $V(1)O_4$ tetrahedra that form the 2D layer. In connectivity terms, the structure may be written as $\{2[V(1)O_{1/1}O_{3/2}]^0\ 3[V(2)O_{1/1}O_{4/2}]^{1-}\}^{3-}$ with charge balance maintained by three A^+ (K^+, Rb^+, or Tl^+) cations. The local coordination environments of V^{5+} and A^+ cations are shown in Supporting Information, Figure S5. The V(1)−O (V(2)−O) bond distances range between 1.617(6)−1.739(3) Å (1.600(6)−1.931(4)Å). As seen in Supporting Information, Figure S5, all three A^+ cations have similar coordination environments. Each A^+ cation is surrounded by 10 oxygen atoms with the A−O bond distances between 2.813(5)−3.338(6) Å (Table 3). The similar coordination environments between the A cation indicate that the lone-pair electrons on the Tl^+ cation are inert, rather than stereochemically active.[76,77] This "inertness" of the lone-pair is in agreement with our DFT and electron localization function (ELF) calculations (see Electronic structure). Bond valence calculations[78,79] resulted in values between 5.03−5.22 for vanadium and 1.11−1.17 for the alkali metals and Tl^+ cation (see Table 4). One of the most interesting features of the $A_3V_5O_{14}$ materials is its topological structural relationship with respect to a layer in the tetragonal tungsten bronze (TTB) topology. Polyhedral representations of a TTB and $A_3V_5O_{14}$ layer are shown in Figure 2. The "A" cations in both structures are shown as green spheres, whereas the d^0 cation polyhedra are in blue, with oxygen atoms in red. With both structures, the "A" cations are surrounded by several polyhedra. In the TTB structure, the "A" cation is surrounded by four or five MO_6 octahedra, whereas in the $A_3V_5O_{14}$ structure the analogous cations are surrounded by five polyhedra, three VO_5 square pyramids and two VO_4 tetrahedra. As a result, the TTB structure has triangular, square, and pentagonal "channels", whereas in $A_3V_5O_{14}$ only triangular and pentagonal "channels" are observed (see Figure 2). The lack of square channels in $A_3V_5O_{14}$ is attributable to the occurrence of the VO_4 tetrahedra. It should be emphasized that the structural relationships between the TTB and $A_3V_5O_{14}$ structures is strictly topological and with respect to the layers only. The TTB structures are three-dimensional, whereas $A_3V_5O_{14}$ exhibits a two-dimensional crystal structure.

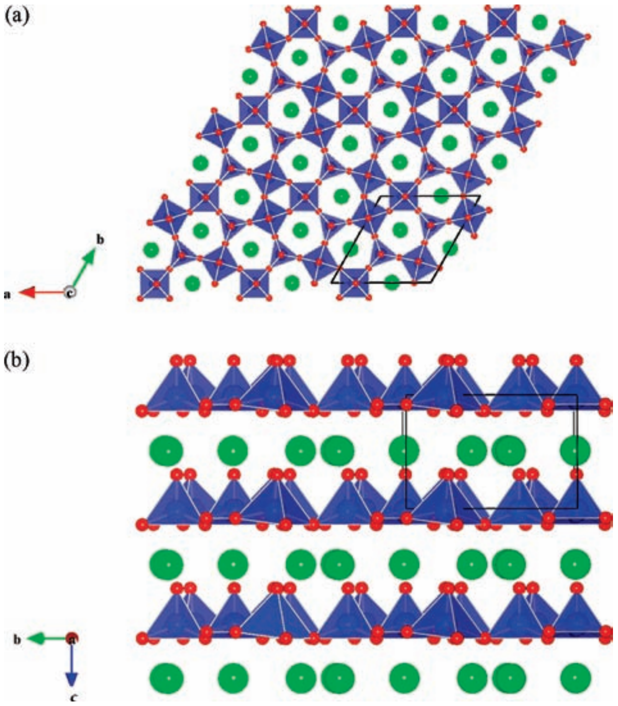

Figure 1. Polyhedral diagram of $A_3V_5O_{14}$ in the (a) *ab*- and (b) *bc*-planes. Note that in (b) all of the polyhedra are pointing in the same direction.

IR Spectroscopy. The IR spectra of $K_3V_5O_{14}$, $Rb_3V_5O_{14}$, and $Tl_3V_5O_{14}$ reveal V−O vibrations between 400 and

---

(74) Baroni, S.; Dal Corso, A.; de Gironcoli, S.; Giannozzi, P.; Cavazzoni, C.; Ballabio, G.; Scandolo, S.; Chiarotti, G.; Focher, P.; Pasquarello, A.; Laasonen, K.; Trave, A.; Car, R.; Marzari, N.; Kokalj, A. http://www.quantum-espresso.org/.

(75) Momma, K.; Izumi, F. *J. Appl. Crystallogr.* **2008**, *41*, 653.

(76) Stoltzfus, M. W.; Woodward, P.; Seshadri, R.; Park, J.-H.; Bursten, B. *Inorg. Chem.* **2007**, *46*, 3839.

(77) Yeon, J.; Kim, S.-H.; Halasyamani, P. S. *J. Solid State Chem.* **2009**, *182*, 3269.

(78) Brown, I. D.; Altermatt, D. *Acta Crystallogr., Sect. B* **1985**, *B41*, 244.

(79) Brese, N. E.; O'Keeffe, M. *Acta Crystallogr., Sect. B* **1991**, *B47*, 192.

Table 3. Selected Bond Distances (Å) for $A_3V_5O_{14}$ (A = K^+, Rb^+, and Tl^+)

$K_3V_5O_{14}$		$Rb_3V_5O_{14}$		$Tl_3V_5O_{14}$	
K(1)−O(1) × 2	2.864(2)	Rb(1)−O(1) × 2	2.925(2)	Tl(1)−O(1) × 2	2.897(3)
K(1)−O(2) × 2	3.156(2)	Rb(1)−O(2) × 2	3.162(4)	Tl(1)−O(2) × 2	3.179(2)
K(1)−O(2)	3.266(5)	Rb(1)−O(2)	3.315(4)	Tl(1)−O(2)	3.338(6)
K(1)−O(3)	2.813(5)	Rb(1)−O(3)	2.983(4)	Tl(1)−O(3)	2.859(5)
K(1)−O(4) × 2	2.873(3)	Rb(1)−O(4) × 2	2.990(2)	Tl(1)−O(4) × 2	2.925(3)
K(1)−O(4) × 2	2.925(3)	Rb(1)−O(4) × 2	3.096(2)	Tl(1)−O(4) × 2	2.992(4)
V(1)−O(1)	1.617(6)	V(1)−O(1)	1.630(4)	V(1)−O(1)	1.635(7)
V(1)−O(4) × 3	1.739(3)	V(1)−O(4) × 3	1.741(2)	V(1)−O(4) × 3	1.747(3)
V(2)−O(2)	1.606(5)	V(2)−O(2)	1.602(4)	V(2)−O(2)	1.600(6)
V(2)−O(3) × 2	1.824(5)	V(2)−O(3) × 2	1.824(4)	V(2)−O(3) × 2	1.825(2)
V(2)−O(4) × 2	1.917(3)	V(2)−O(4) × 2	1.924(2)	V(2)−O(4) × 2	1.931(3)

Table 4. BVS, BSI, and GII Values, Dipole Moments, SHG Efficiencies (Relative to α-SiO_2), Piezoelectric Responses, and Pyroelectric Coefficients for $A_3V_5O_{14}$ (A = K^+, Rb^+, and Tl^+)

	BVS					dipole moments				
compounds	A^+	$V(1)^{5+}$	$V(2)^{5+}$	BSI	GII	$V(1)^{5+}$	$V(2)^{5+}$	SHG	piezo. d_{33} (pm/V)	pyro. coeff. (65 °C, $\mu C/m^2 \cdot K$)
$K_3V_5O_{14}$	1.11	5.22	5.06	0.058	0.103	1.05	1.65	130	28	−2.2
$Rb_3V_5O_{14}$	1.13	5.14	5.05	0.058	0.085	0.90	1.98	80	22	−2.9
$Tl_3V_5O_{14}$	1.17	5.06	5.03	0.059	0.065	1.03	1.87	100	26	−2.8

1000 cm^{-1}. The short terminal V−O (V═O) vibrations are observed in the range of 900−980 cm^{-1}, and the bands occurring at 650−750 cm^{-1} and 400−450 cm^{-1} can be assigned to V−O and V−O−V vibrations, respectively. These assignments are consistent with those previously reported.[48,80−84] The IR spectra and assignments have been deposited in the Supporting Information, Figure S2.

UV−vis Diffuse Reflectance Spectroscopy. All the reported compounds, $K_3V_5O_{14}$, $Rb_3V_5O_{14}$, and $Tl_3V_5O_{14}$ are red. The UV−vis spectra reveal that the absorption energy for all three compounds is approximately 2 eV. Absorption (K/S) data were calculated from the Kubelka−Munk function:[71,72]

$$F(R) = \frac{(1-R)^2}{2R} = \frac{K}{S}$$

with R representing the reflectance, K the absorption, and S the scattering. In a K/S versus E (eV) plot, extrapolating the linear part of the rising curve to zero provides the onset of absorption at 2.11 eV, 2.08 eV, and 1.96 eV for $K_3V_5O_{14}$, $Rb_3V_5O_{14}$, and $Tl_3V_5O_{14}$, respectively. This observation is consistent with the results from our electronic structure calculations. For all three materials, the top of the valence band mainly consists of O-2sp orbitals, whereas the bottom of the conduction band is composed of contributions from V(2)-3d orbitals (major) and V(1)-3d and O-2sp orbitals (both minor). Thus, the optical band gap may be attributed to ligand-to-metal, that is O-2sp to V(2)-3d, charge transfer. The UV−vis diffuse reflectance spectra for the reported compounds have been deposited in the Supporting Information, Figure S3.

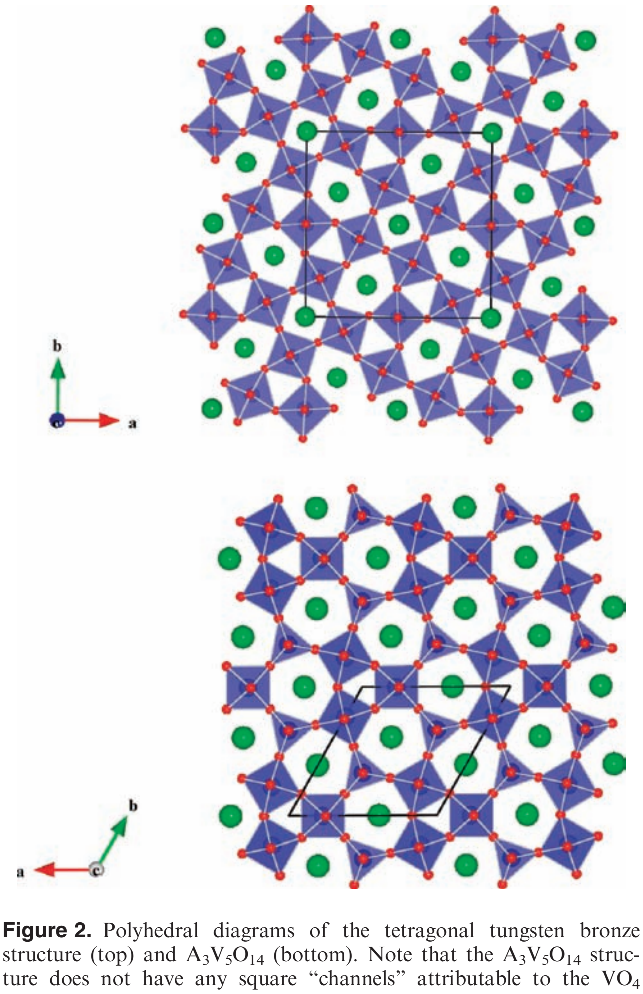

Figure 2. Polyhedral diagrams of the tetragonal tungsten bronze structure (top) and $A_3V_5O_{14}$ (bottom). Note that the $A_3V_5O_{14}$ structure does not have any square “channels” attributable to the VO_4 polyhedra.

Thermal Analyses. The thermal behavior of $K_3V_5O_{14}$, $Rb_3V_5O_{14}$, and $Tl_3V_5O_{14}$ was investigated using thermogravimetric analysis (TGA) and differential scanning calorimetry (DSC). No weight loss was observed up to 900 °C for all the materials. DSC data were collected from RT to 500 °C. The DSC data indicates that $K_3V_5O_{14}$ melts congruently. Transitions are observed at ∼418 °C (∼360 °C) in the heating (cooling) cycle consistent with

---

(80) Devi, R. N.; Vidyasagar, K. *J. Chem. Soc., Dalton Trans.* **1998**, 3013.

(81) Sykora, R. E.; Ok, K. M.; Halasyamani, P. S.; Wells, D. M.; Albrecht-Schmitt, T. E. *Chem. Mater.* **2002**, *14*, 2741.

(82) Frost, R. L.; Erickson, K. L.; Weier, M. L. *Spectrochim. Acta, Part A* **2004**, *60A*, 2419.

(83) Frost, R. L.; Erickson, K. L.; Weier, M. L.; Carmody, O. *Spectrochim. Acta, Part A* **2005**, *61A*, 829.

(84) Sullens, T. A.; Albrecht-Schmitt, T. E. *Inorg. Chem.* **2005**, *44*, 2282.

melting (recrystallization). With $Rb_3V_5O_{14}$, DSC measurements revealed an endothermic peak at ~402 °C during heating, indicating decomposition of $Rb_3V_5O_{14}$ to $RbVO_3$, RbV_3O_8, and $Rb_3V_5O_{14}$. During the cooling cycle, a peak observed at ~353 °C indicates recrystallization of the materials after decomposition. The final residues of $RbVO_3$, RbV_3O_8, and $Rb_3V_5O_{14}$ were confirmed by powder XRD measurements. For $Tl_3V_5O_{14}$, a peak was observed at ~392 °C during heating that indicated decomposition of $Tl_3V_5O_{14}$ to $TlVO_3$ and TlV_3O_8. The additional peak at ~420 °C is thought to be attributable to the melting point of $TlVO_3$.[85] An additional peak at ~346 °C during cooling suggested recrystallization of the materials after decomposition. The final residues of $TlVO_3$ and TlV_3O_8 were confirmed by powder XRD measurements. Powder XRD patterns of the compounds quenched from 450 °C have been deposited to the Supporting Information (see Supporting Information, Figure S6).

Second-Harmonic Generation. Since $K_3V_5O_{14}$, $Rb_3V_5O_{14}$, and $Tl_3V_5O_{14}$ crystallize in the noncentrosymmetric space group, *P*31*m*, SHG measurements were performed. Powder SHG measurements using 1064 nm radiation revealed efficiencies of approximately 130, 80, and 100 × α-SiO_2 for $K_3V_5O_{14}$, $Rb_3V_5O_{14}$, and $Tl_3V_5O_{14}$, respectively, in the 45−63 μm particle size range. Additional SHG measurements, SHG efficiency versus particle size (20−125 μm), revealed that all three compounds are type 1 phase-matchable, and fall into the class C category of SHG materials.[73] On the basis of the SHG efficiency and phase-matching behavior, the average NLO susceptibility $\langle d_{eff} \rangle_{exp}$ may be estimated. The values are 13.1, 10.3, and 11.5 pm/V for $K_3V_5O_{14}$, $Rb_3V_5O_{14}$, and $Tl_3V_5O_{14}$, respectively. These moderate SHG efficiencies may be attributable to alignment of VO_4 and VO_5 polyhedra. As seen in Figure 2, the VO_4 and VO_5 polyhedra are aligned in the same direction. We suggest that this alignment is responsible for the observed SHG efficiencies. It should be noted that although all three reported materials contain V^{5+}, the cations do *not* undergo second-order Jahn−Teller (SOJT) distortions. SOJT distortions in oxides containing d^0 transition metals are observed when the cation is *octahedrally* coordinated.[43] In $K_3V_5O_{14}$, $Rb_3V_5O_{14}$, and $Tl_3V_5O_{14}$, the V^{5+} cations are in tetrahedral and square pyramidal coordination environments. The absence of an out-of-center displacement, that is, SOJT distortion, is likely the reason for the moderate, as opposed to strong, SHG efficiency. We suggest that the earlier reported SHG data for $K_3V_5O_{14}$[64] are erroneously high, and are inconsistent with the structural features of the materials.

Piezoelectric Measurements. Converse piezoelectric measurements were performed on $K_3V_5O_{14}$, $Rb_3V_5O_{14}$, and $Tl_3V_5O_{14}$. With each sample, a maximum voltage of 500 V was applied and 20 measurements were done and averaged. The d_{33} piezoelectric charge constants of 28, 22, and 26 pm/V for $K_3V_5O_{14}$, $Rb_3V_5O_{14}$, and $Tl_3V_5O_{14}$ respectively, were estimated. The piezoelectric data have been deposited in the Supporting Information, Figure S10.

Polarization Measurements. All of the materials are not only noncentrosymmetric but also polar, that is, they possess a permanent dipole moment indicating the possibility of ferroelectric behavior. Although polarization loops were observed that appear similar to ferroelectric hysteresis loops, the materials are *not* ferroelectric.[86] In other words, the macroscopic polarization cannot be switched under an external electric field. The observed polarization "loops" are thought to be attributable to dielectric loss. To understand this irreversibility, the local polarizations in the materials need to be examined. The macroscopic polarity in these compounds is attributable to the local polarity observed in the VO_4 and VO_5 polyhedra. The VO_4 polyhedra, however, exhibit much less polarity, attributable to its tetrahedral coordination environment, compared with the VO_5 polyhedra. For the materials to exhibit ferroelectric behavior, the macroscopic polarization must be "switchable", reversed in the presence of an external electric field. For d^0 transition metals in octahedral oxide coordination environments, it is possible for the cation to be switched from one corner, edge, or face to the opposite, for example, $BaTiO_3$ (corner) and $LiNbO_3$ (face),[87,88] in the presence of an external electric field resulting in ferroelectric behavior. The potentially "switchable" V^{5+} cation is in the VO_5 square pyramids, as the V^{5+} cation in the VO_4 tetrahedra is not in a polar coordination environment. In the VO_5 square pyramid, the dipole moment may be considered switched when the vanadium atom moves toward to the basal plane. This movement is suggested to be energetically unfavorable, as the absence of an axial oxide ligand on the other side of the square pyramid prevents stabilization of the shifted vanadium atom.

Although the reported materials are not ferroelectric, they do exhibit macroscopic polarization indicating the materials are pyroelectric. To determine the pyroelectric coefficient, *p*, the change in polarization as a function of temperature, was measured. The pyroelectric coefficients are −2.2, −2.9, and −2.8 $\mu C/m^2 \cdot K$ for $K_3V_5O_{14}$, $Rb_3V_5O_{14}$, and $Tl_3V_5O_{14}$, respectively, at 65 °C. These values are consistent with other nonferroelectric pyroelectric materials such as ZnO (−9.4 $\mu C/m^2 \cdot K$) and tourmaline (−4.0 $\mu C/m^2 \cdot K$).[1]

Electronic Structure Analysis. We performed electronic structure calculations on $K_3V_5O_{14}$, $Rb_3V_5O_{14}$, and $Tl_3V_5O_{14}$ using pseudopotential methods. Electronic structure calculations have been reported for $K_3V_5O_{14}$.[89] In the published report, the density of states for a wide range of energies, −30 to +5 eV, were examined, whereas we focused on energies above and below the Fermi level, −5 to +5 eV. With our calculations, the total and projected density of states, TDOS and PDOS, respectively, are shown in Figure 3. An energy gap at the Fermi level, indicative of their semiconducting behavior, is observed in the TDOS for each material. The calculated energy gaps are approximately ~2.3 and 2.2 eV and 1.8 eV for $K_3V_5O_{14}$, $Rb_3V_5O_{14}$, and $Tl_3V_5O_{14}$ respectively, consistent with the UV−vis diffuse reflectance data. Overall, their electronic structures are similar. In the PDOSs (see Figure 3), the top of the valence band is mainly composed of O-2sp orbitals, whereas the bottom of the conduction band is composed of V(2)-3d orbitals (major) and V(1)-3d and O-2sp orbitals (both minor). The larger contribution of V(2)-3d relative to V(1)-3d is attributable to the shorter V(1)−O bond compared with V(2)−O.

---

(85) Gaplovska, K.; Zurkova, L. *J. Therm. Anal.* **1981**, *20*, 463.

(86) Scott, J. F. *J. Phys.: Condens. Matter* **2008**, *20*, 021001.

(87) Shirane, G.; Danner, H.; Pepinsky, R. *Phys. Rev.* **1957**, *105*, 846.

(88) Abrahams, S. C.; Hamilton, W. C.; Reddy, J. M. *J. Phys. Chem. Solids* **1966**, *27*, 1013.

(89) Huang, S. P.; Wu, D. S.; Shen, J.; Cheng, W. D.; Lan, Y. Z.; Li, F. F.; Zhang, H.; Gong, Y. J. *J. Phys.: Condens. Matter* **2006**, *18*, 5535.

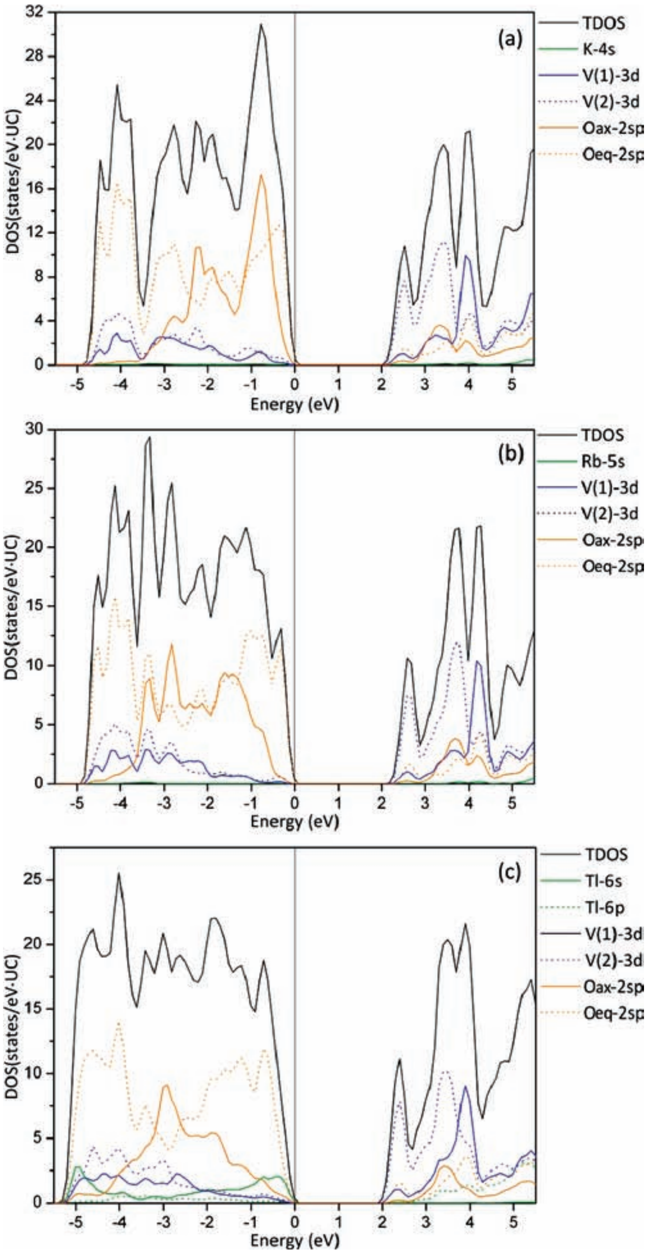

Figure 3. Total and projected density of states for (a) $K_3V_5O_{14}$, (b) $Rb_3V_5O_{14}$, and (c) $Tl_3V_5O_{14}$ calculated using the pseudopotential method.

For $Tl_3V_5O_{14}$ in the PDOSs, attributable to the lone-pair, a small contribution of the Tl-6s orbital is observed at the top of the valence band, whereas the contribution of the Tl-6p orbitals is negligible.

The crystal orbital Hamilton population (COHP) analysis was carried out using the TB-LMTO-ASA method. Figure 4 shows the −COHP curves for the V(1)−O, V(2)−O, and Tl−O bonds in $Tl_3V_5O_{14}$. Bonding and antibonding characteristics of the V−O bonds are observed below and above the Fermi level, respectively. Also, the −COHP curve for the Tl−O reveals the antibonding character near the Fermi level that corresponds to antibonding Tl(6s)−O interactions. Since the Tl-6p orbital contribution into the Tl−O bonds is negligible below the Fermi level, the lone-pair on the Tl^+ cation is anticipated to be highly symmetric, that is, there is negligible mixing between the Tl-6s and -6p orbitals.

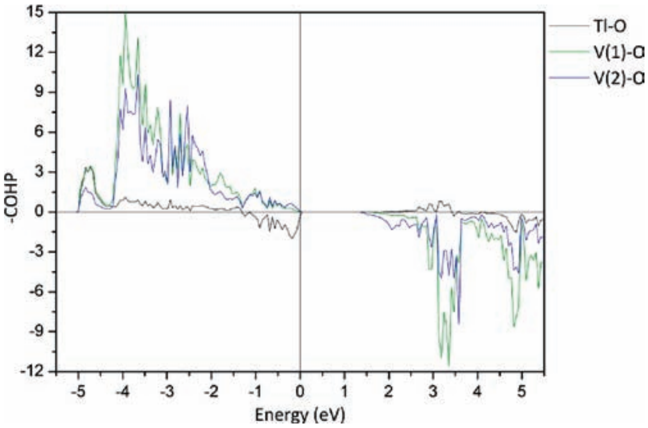

Figure 4. COHP curves for Tl−O, V(1)−O, and V(2)−O in $Tl_3V_5O_{14}$ calculated using the TB-LMTO-ASA method.

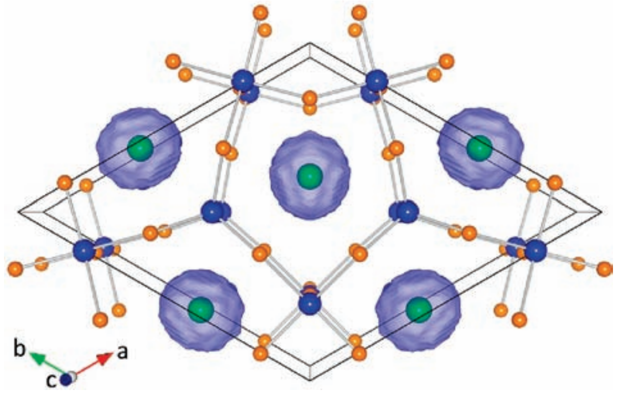

Figure 5. Electron localization function (ELF) isosurface with $\eta = 0.9$ is shown. The sphere-like isosurfaces clearly indicate that the lone-pairs on the Tl^+ cations are inert, as opposed to stereoactive.

To examine the lone-pair character on the Tl^+ cation, electron localization function (ELF) calculations were performed using the TB-LMTO-ASA method. The ELF visualization with $\eta = 0.9$ is shown in Figure 5 where a sphere-like iso-surface is observed at the Tl^+ site. Thus, the lone-pair on Tl^+ may be considered inert, as opposed to stereoactive.[76,77] This indicates that the polarization associated with the Tl^+ is expected to be negligible. Therefore, the polarization associated with all the reported materials is wholly attributable to the vanadium oxide polyhedra.

Local Dipole Moment Calculations. As shown in Supporting Information, Figure S5, we classified the V−O bonds into apex bonds ($V{-}O_{ap}$) along the *c*-direction and equatorial bonds ($V{-}O_{eq}$) in the *ab*-plane. In all three materials, the $V(1)O_4$ tetrahedron has three longer $V(1){-}O_{eq}$ bonds and a shorter $V(1){-}O_{ap}$ bond. Also, the $V(2)O_5$ square pyramid has four longer $V(2){-}O_{eq}$ bonds and a shorter $V(2){-}O_{ap}$ bond. Thus, the geometric center of oxygen atoms in each polyhedron is near the vanadium atom position on each $V{-}O_{ap}$ bond axis parallel to the *c*-axis. Thus, it is expected that the local dipole moments[90,91] associated with the $V(1)O_4$ and $V(2)O_5$ polyhedra are small (see Table 4). Therefore, we anticipate that the macroscopic

---

(90) Debye, P. *Phys. Z.* **1921**, *22*, 302.

(91) Debye, P. *Polar Molecules*; Chemical Catalog Company, Inc.: New York, 1929.

polarization is rather small, consistent with the SHG and polarization measurements.

BSI and GII Indices. Bond strain index (BSI)[92] and global instability index (GII)[93] were calculated (see Table 4). Values of BSI and GII greater than 0.05 vu (valence unit) are indicative of structural strain.[94] The BSI and GII values in Table 4 are substantially above zero indicating the materials exhibit electronic and lattice induced strains. Interestingly, for all materials, GII values are bigger than BSI values, suggesting that the lattice induced strain is stronger than the electronic induced strain. This is not unexpected as none of the cations undergo SOJT distortions. It is interesting to note that although BSI values remain constant among the materials, the GII values *decrease* with *increasing* A cation size, that is, GII ($K_3V_5O_{14}$) > GII ($Rb_3V_5O_{14}$) > GII ($Tl_3V_5O_{14}$). This decrease may be attributable to the differences in the V−O bond distances. The V−O bond distance, on average, *decreases* with *decreasing* A cation size producing a larger amount of lattice strain thereby increasing the GII for the smallest A cation material, $K_3V_5O_{14}$.

Conclusion

Three polar vanadates, $K_3V_5O_{14}$, $Rb_3V_5O_{14}$, and $Tl_3V_5O_{14}$, were synthesized and characterized. All of the materials exhibit a layered crystal structure consisting of TTB-like sheets of corner-shared VO_4 and VO_5 polyhedra. The alkali metal or thallium cations are found between the layers. The materials exhibit moderate SHG efficiencies of ~100 × α-SiO_2. The magnitude of the SHG efficiency can be understood by a close examination of the cation coordination environments. In addition, although all three materials are polar, none are ferroelectric as the polarity associated with the V^{5+} cation, in the VO_4 and VO_5 polyhedra, cannot be reversed. Finally, DSC measurements indicate that $K_3V_5O_{14}$ melts congruently suggesting that large (>5 mm) single crystals could be grown. We are currently in the process of growing such crystals.

Acknowledgment. We thank the Robert A. Welch Foundation (Grant E-1457), the ACS PRF 47345-AC10, and the NSF (DMR-0652150) for support. We also thank the Youngstown State S&CIF X-ray Facility funded by NSF Grant 0087210, Ohio Board of Regents Grant CAP-491, for the single crystal data.

Supporting Information Available: Additional information is provided in Figures S1−S10 and Table S1, and crystallographic data in CIF format. This material is available free of charge via the Internet at http://pubs.acs.org.

---

(92) Preiser, C.; Losel, J.; Brown, I. D.; Kunz, M.; Skowron, A. *Acta Crystallogr., Sect. B: Struct. Sci.* **1999**, *B55*, 698.

(93) Salinas-Sanchez, A.; Garcia-Munoz, J. L.; Rodriguez-Carvajal, J.; Saez-Puche, R.; Martinez, J. L. *J. Solid State Chem.* **1992**, *100*, 201.

(94) Brown, I. D. *The Chemical Bond in Inorganic Chemistry*; Oxford University Press: New York, 2002; Vol. *12*.